CHEMISTRY OF MATERIALS
Cite This: Chem. Mater. 2019, 31, 1057−1065
Article
pubs.acs.org/cm

Defect-Assisted Deposition of Au on Ag for the Fabrication of Core−Shell Nanocubes with Outstanding Chemical and Thermal Stability

Luo Zhang,[†,‡] Yun Zhang,[†] Jaewan Ahn,[†] Xin Wang,[‡] and Dong Qin*[,†]

[†]School of Materials Science and Engineering, Georgia Institute of Technology, Atlanta, Georgia 30332, United States
[‡]School of Material Science and Engineering, Ocean University of China, Qingdao, Shandong 266100, P. R. China

Supporting Information

ABSTRACT: We report the defect-assisted deposition of Au on Ag nanocubes for the generation of Ag@Au core−shell nanocubes with three to eight atomic layers. In a standard protocol, we disperse Ag nanocubes in an ethylene glycol (EG) solution containing poly(vinylpyrrolidone) and then titrate aqueous $HAuCl_4$ at 110 °C. Initially, the galvanic replacement reaction between $HAuCl_4$ and Ag allows the deposition of Au on the edges of the nanocubes with highest surface energy as the Ag atoms on the side faces are dissolved into the aqueous suspension in the form of Ag(I) ions to create surface defects. These defects then become preferential sites for the codeposition of Ag and Au atoms derived from the coreduction of both the Ag(I) and Au(III) ions in the reaction solution by EG. Once the defect sites have been filled, the additional Ag and Au atoms will rapidly diffuse across the entire surface of each nanocube for the generation of a nanocube with a relatively thin shell made of a Ag−Au alloy. Afterward, the chemical reduction of $HAuCl_4$ by EG serves as a predominant pathway to generate Au atoms for their deposition on the nanocubes in a manner similar to conventional seeded growth. We also use surface-enhanced Raman scattering to characterize the transformation of the core−shell nanocubes with a Ag-dominated to a Au-enriched outermost surface as the Au shell thickness is increased. The as-obtained Ag@Au core−shell nanocubes with a Au shell of eight atomic layers are stable in aqueous 30% H_2O_2 for at least 12 h, together with remarkable thermal stability in EG at 110 °C for 6 h.

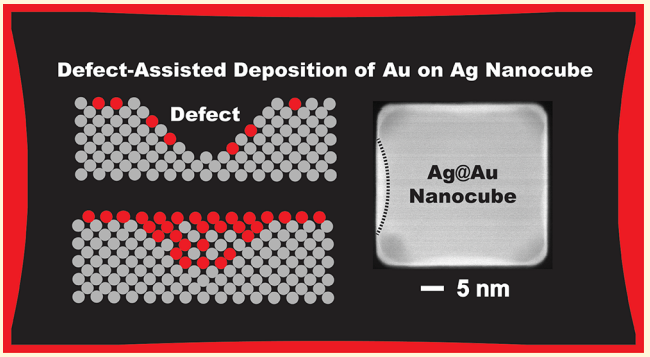

1. INTRODUCTION

Silver nanocrystals have intriguing optical properties for a number of applications related to plasmonics,[1−4] surface-enhanced Raman spectroscopy (SERS),[5−8] and optical sensing.[9,10] However, these applications are plagued by the susceptibility of Ag nanocrystals toward an oxidative environment because of the release of Ag atoms from the high-energy facets. As an example, the Ag nanocubes can only be stored as an aqueous suspension for a few months before they are transformed into truncated nanocubes and then nanospheres. Upon exposure to 3% H_2O_2, these nanocubes will be oxidized instantaneously. One solution to this problem is to enhance the chemical stability of Ag nanocrystals without compromising the unique plasmonic properties of Ag by depositing an ultrathin shell of Au on the surface of Ag nanocrystals for the generation of Ag@Au core−shell nanocrystals.[11] To this end, four different strategies have been demonstrated for fabricating the core−shell nanocrystals. In the first strategy, Yin reported the fabrication of Au-coated Ag nanoplates by using AuI_4^- with a reduction potential lower than that of AuI_4^- to help retard the galvanic replacement reaction between the Au(III) precursor and Ag nanoplates under ambient condition.[12] In the second strategy, Mirkin and Xue documented the deposition of Au on Ag nanoprisms.[13,14] They demonstrated that galvanic replacement and coreduction would allow for the transformation of Ag nanoprisms into nanoprisms made of an Ag−Au alloy, followed by the evolution toward Ag−Au@Au nanoprisms. In the third strategy, Kitaev demonstrated the use of galvanic replacement reaction for the deposition of a uniform shell of Au on the surface of Ag decahedra and pentagonal nanorods in an aqueous system by titrating a very diluted solution of $HAuCl_4$ at an extremely slow rate over a period of 12 h at room temperature.[15] It was argued that the ability to control the concentration of aqueous $HAuCl_4$ to a minimum level could effectively eliminate any possible formation of pits or voids on the surface of Ag nanocrystals, leading to the formation of Ag@Au core−shell nanocrystals.

Most recently, we developed the fourth strategy that enabled the fabrication of Ag@Au core−shell nanocubes by introducing a parallel chemical reduction to compete with and thus suppress the galvanic replacement reaction. In a typical process, aqueous $HAuCl_4$ was titrated into an aqueous suspension of 40 nm Ag nanocubes consisting of ascorbic acid (H_2Asc), NaOH, and poly(vinylpyrrolidone) (PVP) at

Received: November 11, 2018
Revised: January 13, 2019
Published: January 14, 2019

DOI: 10.1021/acs.chemmater.8b04723
Chem. Mater. 2019, 31, 1057−1065

room temperature.[16,17] In this protocol, NaOH played two important roles in controlling the rates of both chemical reduction and galvanic replacement reactions. First, the OH^- would neutralize H_2Asc to generate ascorbate monoanion ($HAsc^-$),[18] a stronger reducing agent, making it possible for the chemical reduction to surpass the galvanic replacement reaction. Second, the OH^- could also neutralize the $HAuCl_4$ to $AuCl_4^-$, which would be further transformed into $AuCl(OH)_3^-$ and $Au(OH)_4^-$ via ligand exchange. These species with lower reduction potentials relative to $AuCl_4^-$ would slow down the galvanic replacement reaction.[19,20] Altogether, it was established that the added Au(III) ions would be reduced predominantly through chemical reduction by $HAsc^-$ to generate Au atoms for their subsequent conformal deposition onto the surface of the Ag nanocrystals in a seeded-growth manner.[21,22]

Despite the successful fabrication of Ag@Au core−shell nanocubes capable of sustaining chemical etching in 2.3% H_2O_2 for 10 h, there are two pitfalls associated with the use of NaOH. First of all, Ag_2O patches are formed at the corners of the Ag@Au core−shell nanocubes because the Ag(I) ions dissolved from the corner sites would react with OH^- for the formation of AgOH and then Ag_2O.[23−25] Second, it was shown that the pH of the reaction solution constantly decreased toward an acidic value when $HAuCl_4$ solution was continuously titrated into the reaction system in an attempt to generate thicker shells of Au on Ag nanocubes. Under acidic condition, together with a large amount of $HAuCl_4$ in the reaction solution, the Ag_2O patches would be dissolved, exposing the underlying Ag to react with $HAuCl_4$ through galvanic replacement reaction in the presence of a relatively weak reducing agent such as H_2Asc.[24] As a result, it still remains a challenge to produce Ag@Au core−shell nanocubes with a shell thickness greater than six atomic layers. Additionally, the utility of the as-obtained core−shell nanocubes with a thin layer of Ag_2O at the corners tends to be compromised because they are still susceptible to an acidic, oxidative environment.

Herein, we report the defect-assisted deposition of Au on Ag nanocubes for the generation of Ag@Au core−shell nanocubes with substantially enhanced chemical and thermal stability by integrating the aforementioned four strategies. Completely different from our previously reported protocol,[16,17,24,26] we redesign the synthetic route by employing ethylene glycol (EG) as both a solvent and a reducing agent to avoid the formation of Ag_2O on Ag nanocrystals by eliminating the involvement of H_2Asc, NaOH, and water. We also perform the synthesis at an elevated temperature, which is completely different from the other three strategies mentioned above.[12−15] In a standard protocol, we disperse Ag nanocubes in an EG solution containing PVP at 110 °C and then slowly titrate aqueous $HAuCl_4$ using a syringe pump. In principle, the added $HAuCl_4$ can be reduced by both EG and Ag via chemical reduction and galvanic replacement reactions. At the early stage of a synthesis, the galvanic replacement reaction between $HAuCl_4$ and Ag creates defects on the {100} facets, or side faces, of the nanocubes, accompanied by the deposition of Au on the surface of Ag nanocubes. As more and more Ag atoms are oxidized from the side faces of nanocubes, the high surface energies associated with the defects make them preferential sites for the codeposition of Ag and Au atoms derived from the reduction of both the Ag(I) ions and Au(III) in the reaction solution by EG. Ultimately, these defect sites are filled with Ag and Au atoms, followed by the rapid diffusion of additional atoms across the surface of each nanocube for the generation of a thin shell made of an Ag−Au alloy. Once the galvanic replacement reaction with Ag is terminated, the added $HAuCl_4$ will be reduced by EG to generate Au atoms, followed by their deposition onto the nanocubes for the generation of Ag@Au core−shell nanocubes with wall thickness up to eight atomic layers. We demonstrate the use of isocyanide as a SERS probe to elucidate the transition of the core−shell nanocubes from an Ag-dominated outermost surface toward an Au-enriched surface when the thickness of the Au shell is increased from 3 to 8 atomic layers. We also establish that the SERS activity of the core−shell nanocubes is stronger than that of Au nanoparticles when excited by a laser in the visible region. We further demonstrate that the Ag@Au core−shell nanocubes with eight atomic layers of Au on the surface embrace both excellent chemical stability in aqueous 30% H_2O_2 for 12 h and an outstanding thermal stability in EG solution at 110 °C for 6 h. Collectively, we believe that the Ag@Au core−shell nanocubes with outstanding chemical and thermal stability would emerge as a practical SERS substrate for chemical and biological detection.

2. EXPERIMENTAL SECTION

2.1. Chemicals and Materials. EG was purchased from J. T. Baker. PVP with an average molecular weight of 55 000 (PVP-55k), sodium hydrosulfide hydrate ($NaHS{\cdot}xH_2O$), silver trifluoroacetate (CF_3COOAg, 98%), aqueous hydrochloric acid (HCl, 37 wt %), acetone, gold(III) chloride trihydrate ($HAuCl_4{\cdot}3H_2O$, 99.9+%), aqueous cetyltrimethylammonium chloride (CTAC, 25 wt %), hydrogen peroxide (H_2O_2, 30 wt % in H_2O), iron(III) nitrate nonahydrate ($Fe(NO_3)_3{\cdot}9H_2O$, 99.95%), aqueous nitric acid (HNO_3, wt 70%), and 1,4-phenylene diisocyanide (1,4-PDI, 97%) were all obtained from Sigma-Aldrich and used as received. Deionized water with a resistivity of 18.2 MΩ·cm at 25 °C was used in all the of experiments.

2.2. Synthesis of Silver Nanocubes. We followed a published protocol for the synthesis of Ag nanocubes with an average edge length of 37.5 ± 1.3 nm.[27] The as-obtained Ag nanocubes were washed with acetone and water once each and then redispersed in water for further use. The suspension of Ag nanocubes had a concentration of 1.21×10^{13} particles/mL.

2.3. Synthesis of Ag@Au Core−Shell Nanocubes. We prepared aqueous $HAuCl_4$ (0.1 mM) and left the solution in a refrigerator for 2 weeks before use. In a typical synthesis, we introduced 22.5 μL of the aqueous suspension of Ag nanocubes (approximately 2.7×10^{11} particles in total) into 3.5 mL of EG solution containing 0.05 g of PVP-55k in a 23 mL glass vial under magnetic stirring at 110 °C. Next, we titrated 1.0 mL of the aqueous $HAuCl_4$ into the mixture using a syringe pump at a rate of 4 $mL{\cdot}h^{-1}$ in 11 rounds of titration. Specifically, we started with two consecutive rounds of titration at a titration volume of 0.05 mL for each round, followed by nine rounds at a titration volume of 0.1 mL. We allowed the reaction to proceed for 10 min after each round of titration. We then titrated additional 3.0 mL of aqueous $HAuCl_4$ into the reaction solution in six rounds at a titration volume of 0.5 mL for each round. Finally, we quenched the reaction in ice bath and washed the solid products with 40 mL of acetone once (8000 rpm, 15 min) and 1 mL of water twice (4000 rpm, 20 min). The final products were redispersed in water for future use. The particles were washed with 2 mM aqueous CTAC solution once prior to transmission electron microscopy (TEM) characterization in an effort to obtain a closely packed array of particles for TEM imaging at different magnification.[28]

2.4. Etching of the Ag@Au Core−Shell Nanocubes. We collected the solid products by centrifugation at 4000 rpm for 20 min and then added 1 mL of aqueous H_2O_2 (30 wt %) or 1 mL of aqueous

DOI: 10.1021/acs.chemmater.8b04723
Chem. Mater. 2019, 31, 1057−1065

$Fe(NO_3)_3$ (0.05 mM in 1 wt % aqueous HNO_3). Afterward, we sonicated the centrifuge tubes for a few seconds before the mixture was in idle for 12 h. The solid products were collected through a centrifugation process at 6000 rpm for 15 min and then washed with water once. The particles were also washed with 2 mM aqueous CTAC solution once prior to TEM characterization.[28]

2.5. Synthesis of Au Nanospheres. We followed a published protocol for the synthesis of Au nanospheres with an average diameter of 53.9 ± 1.7 nm.[29] The as-obtained Au nanospheres were washed with water once and then redispersed in water for further use.

2.6. SERS Measurements. The as-obtained Ag@Au core−shell nanocubes were functionalized with 1,4-PDI (10^{-4} M in ethanol) for 2 h. Upon washing with water twice, the nanoparticles were redispersed in 0.2 mL of water to attain a concentration of $\sim 10^{10}$ particles per mL. In a standard SERS measurement, we added 20 μL of the solution to a poly(dimethylsiloxane) cell. We recorded the SERS spectra using a Renishaw inVia Raman spectrometer coupled with a Leica microscope with a 100× objective lens. Other experimental parameters include laser excitation wavelength at 532 nm with an output power of 50 mW, a notch filter based on a grating of 2400 lines/mm, and the collection time was 10 s.

2.7. Instrumentation and Characterization. We used an Eppendorf 5430 centrifuge for the collection of solids and washing of nanoparticles. We used a Cary 50 spectrometer (Agilent Technologies, Santa Clara, CA) to record UV−vis spectra. We used a NexION 300Q ICP−MS (PerkinElmer, Waltham, MA) to measure the Au and Ag contents in the nanocrystals. We used a Renishaw inVia Raman spectrometer (Wotton-under-Edge, U.K.) integrated with a Leica microscope (Wetzlar, Germany) to record Raman spectra. We used A Hitachi HT7700 microscope (Hitachi, Tokyo, Japan) operated at 120 kV to take TEM images. We used a Hitachi HD2700 C_s-corrected microscope operated at 200 kV to collect high-angle annular dark-field scanning TEM (HAADF-STEM) images. We used the energy-dispersive X-ray (EDX) detector on the HD2700 to create elemental mapping of the nanocrystals.

3. RESULTS AND DISCUSSION

In a typical synthesis, we dispersed the Ag nanocubes in an EG solution containing PVP and heated it to 110 °C, followed by the titration of aqueous $HAuCl_4$ (0.1 mM) using a syringe pump at a rate of 4 mL·h^{-1}. Figure 1 illustrates the pathway proposed to account for the transformation of an Ag nanocube into an Ag@Au core−shell nanocube through multiple rounds of titration. Each round consists of the titration of $HAuCl_4$ solution and an idle period of 10 min afterward. In the first step, we titrated two consecutive rounds by introducing 0.05 mL of aqueous $HAuCl_4$ per round into the reaction solution. Because a galvanic reaction would occur instantaneously when Ag nanocubes were mixed with $HAuCl_4$ in an aqueous solution under ambient condition,[30,31] the added 0.1 mL of $HAuCl_4$ could be predominantly reduced by Ag via the galvanic replacement reaction at 110 °C. As reported in our previous work,[32] preferential capping of PVP to the {100} facets of Ag nanocubes in EG would initiate the oxidation of Ag atoms from the side faces to create defects as the deposition of Au would progress on the orthogonal sites such as edges and corners. In the second step, we conducted nine consecutive rounds of titration by adding 0.1 mL of aqueous $HAuCl_4$ during each round. As more $HAuCl_4$ was involved in the reaction solution, the galvanic replacement reaction would become more significant, leading to the dissolution of more Ag atoms into the reaction solution in the form of Ag(I) ions. Concurrently, the released Ag(I) ions and the remaining $HAuCl_4$ in the reaction solution could be coreduced by EG for the generation of Ag and Au atoms, respectively, followed by their codeposition in the form of Ag−Au alloy on the defect

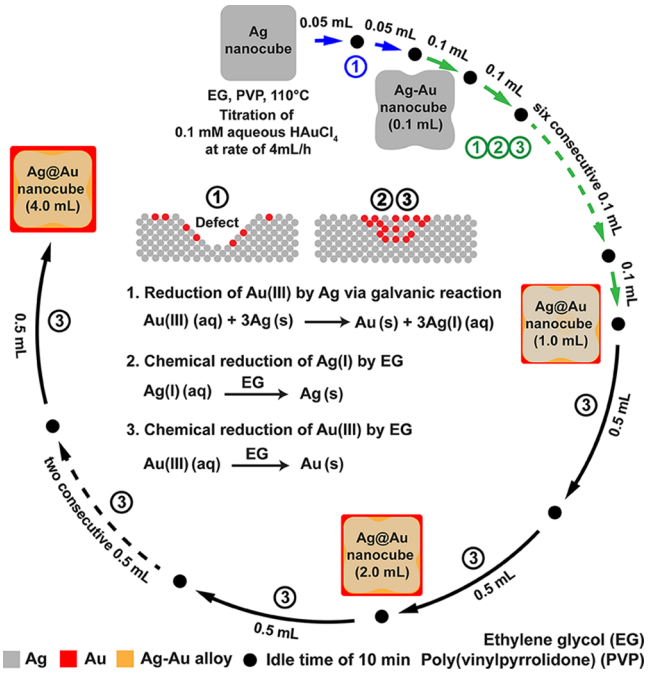

Figure 1. Schematic illustration of a multiple-round titration process used for the transformation of Ag nanocubes into Ag@Au core−shell nanocubes in a PVP/EG solution at 110 °C.

sites (due to their high surface energies) to fill the pits before diffusing across the surface of the nanocubes. At a total titration volume of 1.0 mL, such a thin and conformal shell of Ag−Au would be deposited on the entire surface of the Ag nanocubes, suppressing the galvanic replacement reaction between Ag and $HAuCl_4$. In the third step, we titrated six additional rounds of 0.5 mL of aqueous $HAuCl_4$, during which the newly added precursor would be reduced by EG to generate Au atoms for their deposition on the Ag@Au nanocubes in a manner similar to seeded growth. Taken together, we could adjust the injection rates of aqueous $HAuCl_4$ for different rounds of titration to control the concentration of $HAuCl_4$ in the reaction solution, making it feasible to favorably manipulate the rate of chemical reduction by EG relative to galvanic replacement reaction. This approach is completely different from those reported in the literature that involved the use of an aqueous system to synthesize Ag−Pd or Ag−Au hollow nanoparticles by leveraging galvanic replacement and codeposition.[31,33]

During a synthesis, we could use UV−vis spectroscopy to follow the reaction by comparing the localized surface plasmon resonance (LSPR) spectra of the Ag nanocubes before and after reacting with different volumes of 0.1 mM aqueous $HAuCl_4$. Figure 2A shows that the major LSPR peak of the Ag nanocubes was shifted from 445 to 453, 458, and 460 nm at a total titration volume of 0.2, 0.4, and 0.6 mL, respectively, together with a subtle decrease in intensity. We also used electron microscopy to characterize the morphology of the products in detail. Figure 2B−D shows TEM images of the Ag nanocubes before and after reacting with 0.2 and 0.6 mL of $HAuCl_4$, respectively. At 0.2 mL, we were able to resolve a distinctive red shift in the major LSPR peak from 445 to 453 nm. Such a red shift in the major LSPR peak would suggest the reaction between Ag nanocubes and $HAuCl_4$. However, we did not observe the formation of defects, that is, pits or voids, on the nanocubes when a conventional TEM was used (Figure

DOI: 10.1021/acs.chemmater.8b04723
Chem. Mater. 2019, 31, 1057−1065

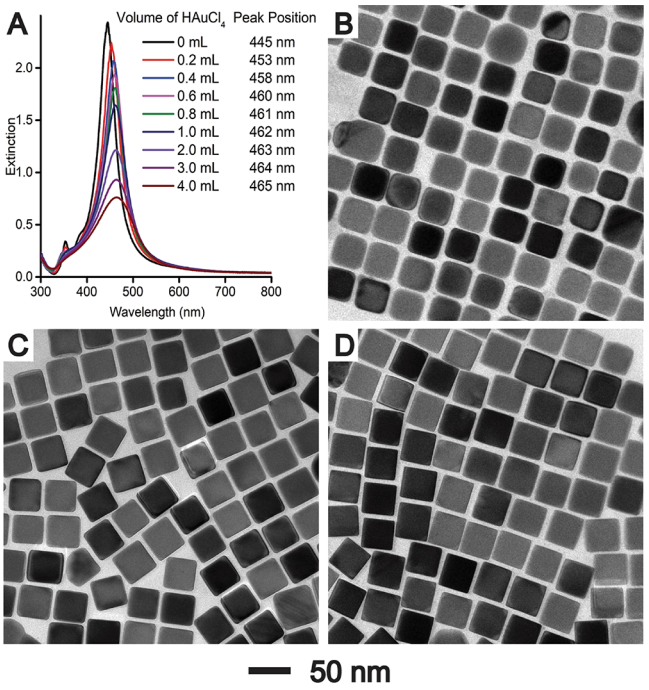

Figure 2. (A) UV−vis spectra of Ag nanocubes before and after reacting with different volumes of aqueous $HAuCl_4$ in a PVP/EG solution at 110 °C. TEM images of (B) Ag nanocubes before and after reacting with (C) 0.2 and (D) 0.6 mL of aqueous $HAuCl_4$.

2C). When compared with the morphology of Ag nanocubes (Figure 2B), the as-obtained sample showed less truncation at the corners, with an average edge length close to the original Ag nanocubes at 37.5 ± 1.3 nm. At 0.6 mL, there was no obvious change in morphology while the average edge length of the nanocubes was increased to 38.3 ± 1.0 nm.

When the titration volume of $HAuCl_4$ was further increased from 0.6 to 0.8, 1.0, 2.0, 3.0, and 4.0 mL, Figure 2A shows that the major LSPR peak was only shifted from 460 to 461, 462, 463, 464, and 465 nm, respectively. It is worth mentioning that the decrease in peak intensity mainly arose from the dilution effect because of the increase in the titration volume. The slight change in peak position suggests that the structure or morphology of the as-obtained nanocubes was largely unaltered. These results also suggest that the deposition of such a thin Au shell should not lead to any significant change to the dielectric constant of Ag, and as a result, the Ag@Au nanocubes exhibited LSPR properties that are essentially identical to those of the Ag nanocubes. Figure 3A−D shows TEM images of the samples obtained at total titration volumes of 1.0, 2.0, 3.0, and 4.0 mL. Again, there were no pits or voids on the nanocubes, but their average edge lengths were further increased to 39.7 ± 1.5, 40.5 ± 1.5, 41.2 ± 1.0, and 41.8 ± 1.5 nm.

To confirm the deposition of Au atoms on the surfaces of the Ag nanocubes, we used etchants based on H_2O_2 and $Fe(NO_3)_3/HNO_3$, respectively, to selectively remove Ag but not Au. Figure S1A,B, shows TEM images of the as-obtained Ag−Au nanocubes prepared with 0.1 mL of aqueous $HAuCl_4$ and the resultant structures after etching with 5% aqueous H_2O_2 for 12 h. Although there were no voids on the Ag−Au nanocubes, we observed the formation of nanoframes upon the removal of Ag, suggesting that the galvanic replacement reaction between $HAuCl_4$ and Ag resulted in the initial deposition of Au on the edges of the nanocubes. Figure 3E−H, shows TEM images of the samples shown in Figure 3A−D, after etching with 30% H_2O_2 for 12 h. We noticed very little change in morphology. In comparison, Figure 3I−L, shows TEM images of the samples after etching with 0.05 mM $Fe(NO_3)_3/HNO_3$ solution for 12 h. Because $Fe(NO_3)_3$ could selectively remove Ag from an Ag−Au alloy, we observed the formation of nanoframes with holes at corners and nanoboxes with openings at corners for the samples obtained with 1.0 and 2.0 mL of $HAuCl_4$. When the titration volume was increased to

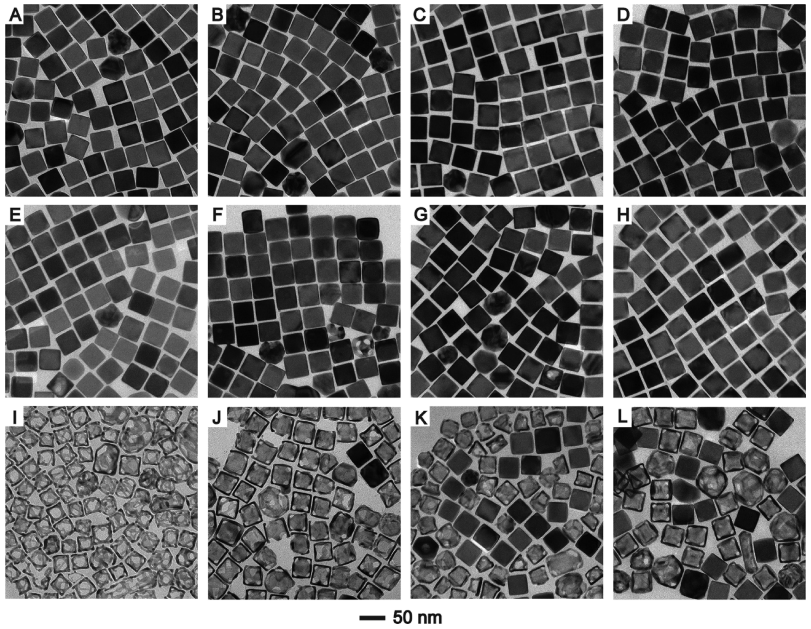

Figure 3. TEM images of Ag@Au core−shell nanocubes prepared by reacting Ag nanocubes with titration volumes of aqueous $HAuCl_4$ at (A) 1.0, (B) 2.0, (C) 3.0, and (D) 4.0 mL. (E−H) TEM images of the resultant structures after etching the samples in (A−D) with 30% H_2O_2. (I−L) Resultant structures after etching the samples in (A−D) with 0.05 mM $Fe(NO_3)_3/HNO_3$.

DOI: 10.1021/acs.chemmater.8b04723
Chem. Mater. 2019, 31, 1057−1065

3.0 and 4.0 mL, we noticed that some nanocubes were able to survive the etching process. Taken together, our results suggest that the edges and side faces of the nanocubes were covered by a thicker layer of Au while the corner sites were covered by an Ag−Au alloy. Remarkably, these newly developed Ag@Au core−shell nanocubes embrace enhanced chemical stability when compared with our previously reported Ag@Au core−shell nanocubes with Ag_2O at the corners.[16,24] In the latter case, Ag_2O would be dissolved by 30% H_2O_2 or HNO_3, making the underneath Ag susceptible to etching.

It is worth mentioning that the preparation of the aqueous $HAuCl_4$ played an essential role in ensuring a successful synthesis. In the standard protocol, we first prepared a 10 mM aqueous solution of $HAuCl_4$ and then stored it in a refrigerator for 14 days. Next, we diluted the aged solution to obtain 0.1 mM aqueous $HAuCl_4$ used for the synthesis of Ag@Au nanocubes. In contrast, when we used freshly prepared 0.1 mM aqueous $HAuCl_4$ while reusing all other experimental parameters, we noticed the creation of Ag−Au nanocubes with pits on the side faces (Figure S2), suggesting the significant involvement of galvanic replacement. We tried to use UV−vis spectroscopy to characterize the aged and freshly prepared aqueous $HAuCl_4$. However, as shown in Figure S3, we could not tell any difference between these two solutions. We argue that the aged aqueous $HAuCl_4$ would allow for the generation of other Au(III) species such as $HAu(OH)_nCl_{(4-n)}$ (n = 1−2) with lower reduction potentials via ligand exchange between Cl^- and H_2O, making it possible for chemical reduction to compete with and thereby inhibit the galvanic replacement reaction effectively for the transformation of Ag nanocubes into Ag@Au core−shell nanocubes.[17,19,20]

We used aberration-corrected HAADF-STEM to characterize the Ag@Au nanocubes. Figure 4A,C shows HAADF-STEM images of two samples prepared with 1.0 and 4.0 mL of $HAuCl_4$. On the basis of the contrast between Au and Ag arising from their difference in atomic number, we clearly observed a nanocube with an Ag core and a thin shell made of Au. In Figure 4A, we were able to identify defects (marked by dotted black line) on the side faces of the Ag nanocubes, at which Au atoms would be deposited to fill the cavities first before the conformal deposition of Au was continued across the entire surface of a nanocube for the generation of a core−shell nanocube (see Figure 4B). These results validate our hypothesis that the galvanic replacement reaction between Ag nanocubes and $HAuCl_4$ would account for the creation of these defects at the early stage of a synthesis, which is consistent with the red shift in the LSPR peak of Ag nanocubes as shown in Figure 2A. When the nanocube was titled to the [001] zone axis, Figure 4B,D shows atomic-resolution HAADF-STEM images to reveal details of the atomic arrangement for the columns of Au and Ag atoms. On average, three and eight atomic layers of Au were deposited on the Ag nanocubes when the titration volumes of $HAuCl_4$ were 1.0 and 4.0 mL.

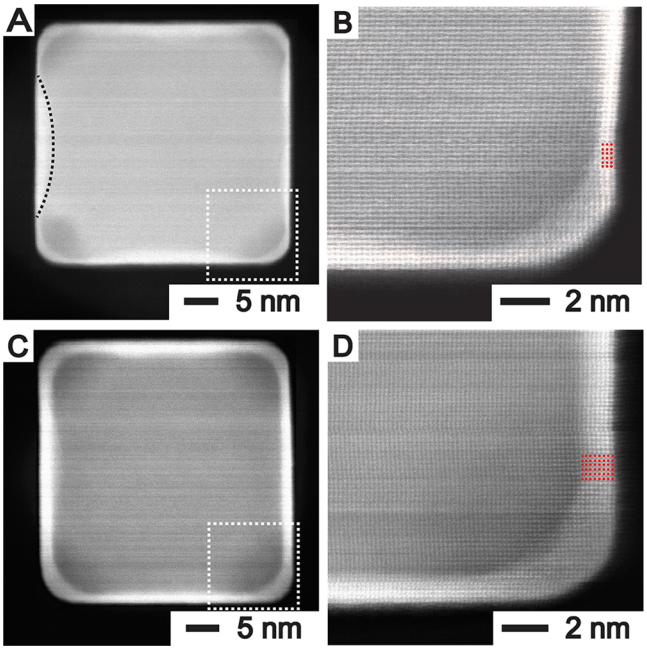

Figure 4. HAADF-STEM images of two samples prepared by reacting Ag nanocubes with (A,B) 1.0 and (C,D) 4.0 mL of aqueous $HAuCl_4$ in EG solution containing PVP at 110 °C.

We also analyzed two samples using HAADF-STEM and EDX. Figure 5A,D shows HAADF-STEM images of two individual nanocubes prepared with titration volume of 1.0 and 4.0 mL for the $HAuCl_4$ solution. When the particle was oriented along the [001] zone axis, Figure 5B,C gives the elemental mapping of Ag and Au for the same cube shown in Figure 5A, while Figure 5E,F shows the elemental mapping of Ag and Au for the same cube shown in Figure 5D. These results confirm that the Ag core remained in a cubic shape and the deposition of Au led to thicker layers on the edges relative to those on the side faces.

To further support our hypothesis that Ag dissolved from the side faces of nanocubes via galvanic replacement reaction would be coreduced with $HAuCl_4$ by EG, followed by the codeposition of Ag and Au atoms onto the nanocubes, we used inductively coupled plasma mass spectrometry (ICP−MS) to measure the mass of Au and Ag in the as-prepared samples when different volumes of 0.1 mM $HAuCl_4$ were involved in the standard protocol. Specifically, we used a centrifugation to collect two samples, solids and supernatants, followed by ICP−MS analyses to separately determine their Au and Ag contents. Figure 6A indicates that the amount of gold in the solid samples linearly increased from 16.2 to 60.2 μg when the titration volume of added $HAuCl_4$ was increased from 1.0 to 4.0 mL. By assuming that the added $HAuCl_4$ was completely reduced to Au atoms for their deposition onto the Ag nanocubes, Figure 6A also shows the calculated values of Au in the solids at different titration volumes (the solid line), close to the experimental values. These results confirm that the $HAuCl_4$ added into the reaction solution was, indeed, completely converted into Au atoms for their deposition onto the Ag nanocubes. Figure 6B shows that the amount of Ag in solids was sustained at the initial value of 152.2 μg during the titration from 1.0 to 4.0 mL of $HAuCl_4$. Because the Ag content in the supernatant was below the detection limit in the course of the synthesis, we believe that there was little loss of Ag from the nanocubes. This result suggests that EG could reduce the Ag(I) ions released from nanocubes to generate Ag atoms for their redeposition back to nanocubes.

It should be pointed out that we did not observe any self-nucleation for Au when following the standard protocol up to 4.0 mL of $HAuCl_4$. We argue that the multiple-round titration process was effective in controlling the concentration of $HAuCl_4$ for the elimination of self-nucleation, making it feasible to deposit eight atomic layers of Au on the Ag

DOI: 10.1021/acs.chemmater.8b04723
Chem. Mater. 2019, 31, 1057−1065

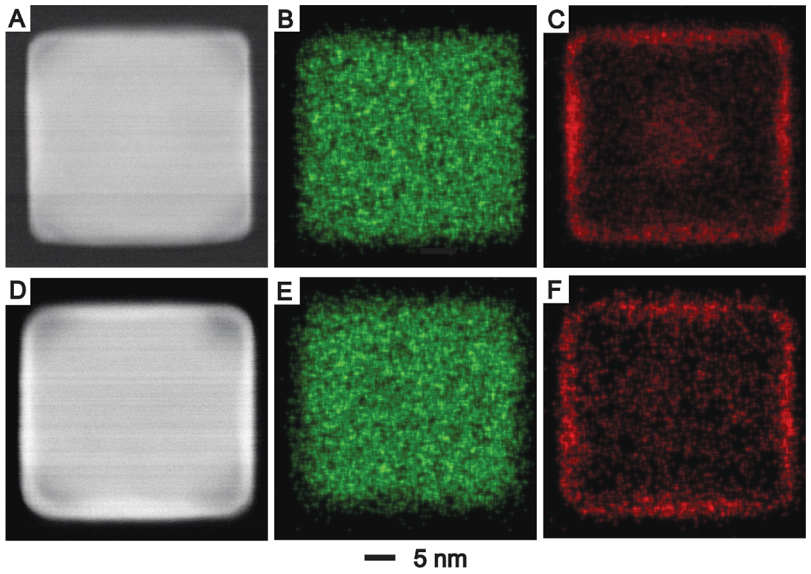

Figure 5. (A,D) HAADF-STEM image of Ag@Au core−shell nanocubes prepared by reacting Ag nanocubes with 1.0 and 4.0 mL of aqueous 0.1 mM $HAuCl_4$ in EG solution containing PVP at 110 °C. (B,C) EDX elemental mapping of an individual nanocube shown in (A) (green, Ag; red, Au). (E,F) EDX elemental mapping of an individual nanocube shown in (D) (green, Ag; red, Au).

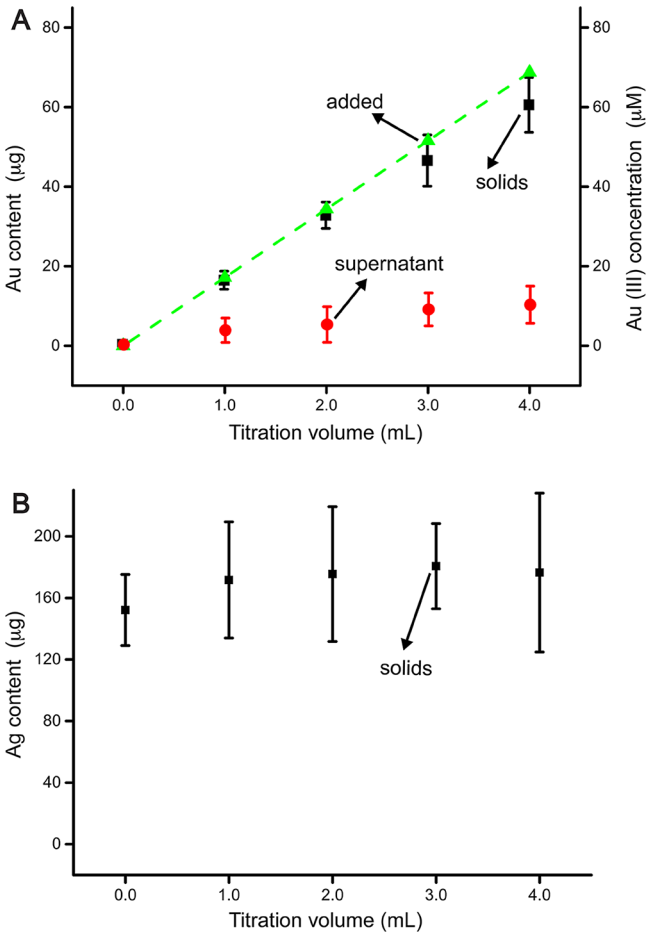

Figure 6. ICP−MS data of (A) Au and (B) Ag for the corresponding products (solids and supernatant) prepared by titrating $HAuCl_4$ into a suspension of Ag nanocubes in EG containing PVP. The data points labeled as "added" correspond to the amounts of Au calculated under the assumption of complete reduction for the added $HAuCl_4$, followed by the deposition of the Au atoms onto the Ag nanocubes.

nanocubes. However, we found that self-nucleation of Au atoms derived from the reduction of $HAuCl_4$ by EG would occur when the titration volume was further increased from 4 to 6 or 8 mL. Figure S4 shows TEM images of the as-obtained Ag−Au nanocubes, from which we clearly identify the Au nanoparticles formed through self-nucleation. We also noticed that the edge length of the Ag−Au nanocubes was slightly increased from 41.8 ± 1.5 nm for those prepared with 4 mL of $HAuCl_4$ to 42.0 ± 1.9 and 42.4 ± 1.5 nm, respectively, for the 6 and 8 mL sample. These results suggest that one needs to refine the standard protocol to deposit more than eight atomic layers of Au on Ag nanocubes. At larger titration volumes of $HAuCl_4$, we argue that $HAuCl_4$ would be accumulated in the solution, leading to an increase in reduction rates and thus the concentration of Au atoms toward self-nucleation.

Although both the STEM and ICP−MS results indicate that Ag would be oxidized from side faces of nanocubes to create defects for the codeposition of Au and Ag atoms, it remains unclear how to characterize the composition of the outmost surface layer of the nanocubes during the titration process using STEM and EDX. To this end, we used 1,4-PDI as a molecular probe to detect the binding of isocyanide group to the outermost surface of Ag@Au core−shell nanocubes by SERS.[34,35] We hypothesize that the stretching frequency of NC bond would be different when lone-pair electrons of carbon bind to Ag or Au atoms on the surface of a nanocube.[36] Figure 7 shows the SERS spectra of 1,4-PDI adsorbed on Ag nanocubes, Ag@Au nanocubes prepared with different titration volumes of $HAuCl_4$ solution, and Au nanospheres at an excitation wavelength of 532 nm. The Au nanospheres (Figure S5) were synthesized by following a published protocol.[29] For Ag nanocubes, the peak located at 2172 cm^{-1} can be assigned to the NC stretching, ν_{NC} band, whereas the three peaks located 1599, 1200, and 1163 cm^{-1} are associated with the ν_{CC}, ν_{CNC}, and ν_{CH} bands of 1,4-PDI, respectively. We noticed that the ν_{NC} band was positioned at 2172 cm^{-1} for the two samples of Ag@Au nanocubes prepared with 1.0 and 2.0 mL of $HAuCl_4$ solution. As the titration volume was increased to 3.0 mL, the ν_{NC} peak was blue-shifted

DOI: 10.1021/acs.chemmater.8b04723
Chem. Mater. 2019, 31, 1057−1065

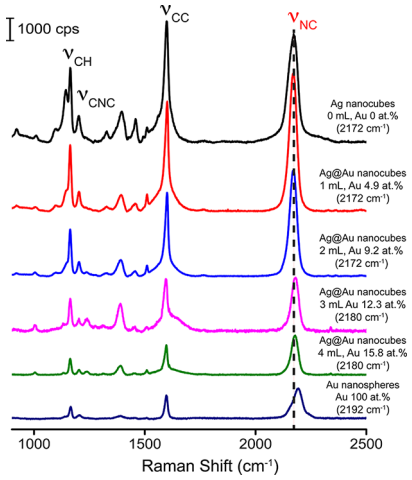

Figure 7. SERS spectra of the 1,4-PDI-functionalized Ag nanocubes, Ag@Au nanocubes prepared at different titration volumes of aqueous $HAuCl_4$, and Au nanospheres.

from 2172 to 2180 cm^{-1} and this peak remained at 2180 cm^{-1} for the sample prepared with 4.0 mL of $HAuCl_4$ solution. We also collected the SERS spectrum from 1,4-PDI-functionalized Au nanospheres, in which the peak position of ν_{NC} band was located at 2192 cm^{-1}. It is worth mentioning that we did not observe the free ν_{NC} band of 1,4-PDI that should be located at 2130 and 2125 cm^{-1} for Ag and Au surfaces, respectively.[34] This result suggests that the 1,4-PDI detected by SERS were likely trapped between two nanoparticles for the generation of hot spots and thus substantial enhancement in SERS signal. Taken together, we argue that there was a transformation from an Ag-dominated surface to an Au-enriched surface when the titration volume of $HAuCl_4$ was augmented from 1 to 4 mL, consistent with the $Fe(NO_3)_3/HNO_3$ etching results. Additionally, we demonstrated that the Ag@Au core−shell nanocubes exhibited much stronger SERS activity when compared with the Au nanospheres in the visible region, making the core−shell nanocubes a better alternative to Au nanoparticles in terms of both SERS activity and chemical stability.

We also demonstrated excellent thermal stability for the Ag@Au core−shell nanocubes. In an evaluation process, we collected the solid from the sample prepared with 4.0 mL of aqueous $HAuCl_4$, redispersed them in 1 mL of EG host in a 23 mL vial and placed it in an oil bath held at 110 °C for 6 h. Figure 8A shows the TEM of the sample after the thermal treatment. We found that the morphology of the nanocubes remained essentially the same as those shown in Figure 3D, showing almost no change after heating at 110 °C for 6 h. We also collected UV−vis spectra from samples before and after the thermal stability test. As shown in Figure 8B, the spectra did not change at all, indicating that the as-obtained Ag@Au core−shell nanocubes were stable in EG solution held at 110 °C. In comparison, Figure S6A shows the morphology of Ag nanocubes after following the same thermal treatment for 6 h, indicating the formation of Ag nanocubes into nanospheres. We also recorded UV−vis spectra of the Ag nanocubes before and after thermal treatment of 2, 4, and 6 h. Figure S6B shows that the LSPR peak of Ag nanocubes was blue-shifted from 445 to 426, 422, and 420 nm, consistent with TEM result. As a result, we believe that the Ag@Au core−shell nanocubes with

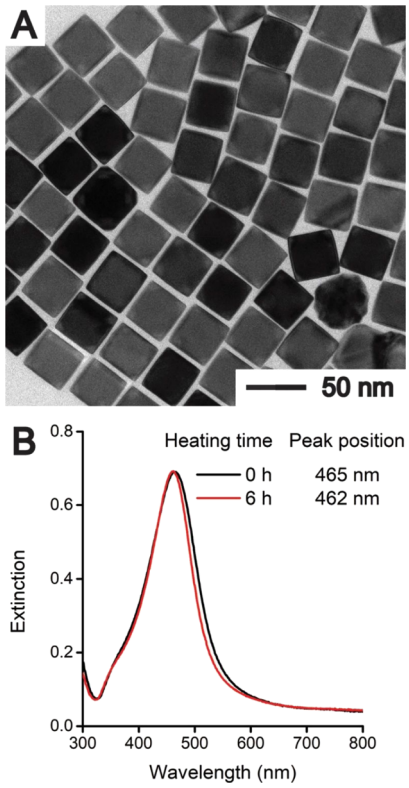

Figure 8. (A) TEM image of the resultant structures after the sample shown in Figure 3D had been incubated in EG at 110 °C for 6 h. (B) UV−vis spectra of the sample before and after the thermal treatment in EG at 110 °C.

an Au shell of eight atomic layers embrace greatly enhanced thermal stability.

4. CONCLUSIONS

We have demonstrated the defect-assisted deposition of Au on Ag nanocubes for the generation of core−shell nanocubes with enhanced chemical and thermal stability. In a typical synthesis, we dispersed Ag nanocubes in an EG solution containing PVP, followed by heating to 110 °C and multiple-round titration of aqueous $HAuCl_4$ using a syringe pump. Our success relies on the ability to control the instantaneous concentration of $HAuCl_4$ in the reaction solution and thus the relative reduction rates of $HAuCl_4$ by Ag and EG via galvanic replacement reaction and chemical reduction, respectively. In the early stage, the galvanic replacement reaction between $HAuCl_4$ and Ag would create defects on the side faces of nanocubes because of the selective binding of PVP to the {100} facets on Ag nanocubes. Concurrently, the released Ag(I) ions and the remaining $HAuCl_4$ in the reaction solution were coreduced by EG for the generation of Ag and Au atoms, respectively, followed by their preferential codeposition on the defect sites in the form of Ag−Au alloys. Once the defects had been filled, these deposited atoms would start to migrate across the surface of the nanocubes via surface diffusion, leading to the generation of a shell made of Ag−Au alloys on the Ag nanocubes. Afterward, the galvanic replacement reaction would be largely terminated, making the chemical reduction of $HAuCl_4$ by EG a predominant pathway to generate Au atoms for their deposition on the nanocubes in a manner similar to seeded growth. By simply changing the titration volume of aqueous $HAuCl_4$, we were able to manipulate the Au shell

DOI: 10.1021/acs.chemmater.8b04723
Chem. Mater. 2019, 31, 1057−1065

thickness from three to eight atomic layers. As the thickness of the shell was increased, we observed the transition from an Ag-dominated toward an Au-enriched outermost surface for the core−shell nanocubes. The Ag@Au core−shell nanocubes with an Au shell of eight atomic layers embraced excellent chemical stability in aqueous 30% H_2O_2 for at least 12 h, as well as outstanding thermal stability in EG held at 110 °C for up to 6 h. We believe that this synthetic strategy has the potential to be extended to other noble metals such as Pd, Pt, and Ir for the fabrication of core−shell bimetallic nanocrystals with plasmonic properties similar to those of Ag but with greatly improved stability and diversified surface and catalytic properties.

■ ASSOCIATED CONTENT

Supporting Information

The Supporting Information is available free of charge on the ACS Publications website at DOI: 10.1021/acs.chemmater.8b04723.

TEM image of Ag−Au nanocubes prepared by 0.1 mL of aged 0.1 mM aqueous $HAuCl_4$ and the resultant structures after etching with 5% H_2O_2, TEM images of Ag−Au nanocubes prepared by reacting the Ag nanocubes with 1, 2, 3, 4 mL of the freshly prepared 0.1 mM aqueous $HAuCl_4$, UV−vis spectra of 0.1 mM aqueous $HAuCl_4$ that were diluted from the 10 mM aqueous $HAuCl_4$ prepared 14 days ago and the one prepared freshly, TEM images of Ag−Au nanocubes prepared by reacting Ag nanocubes with 6 and 8 mL of the aged 0.1 mM aqueous $HAuCl_4$, TEM image of Au nanospheres, and TEM image of the resultant structures of Ag nanocubes after incubation in an oil bath held at 110 °C for 6 h and the corresponding UV−vis spectra of the sample before and after the thermal treatment for different periods of time (PDF)

■ AUTHOR INFORMATION

Corresponding Author

*E-mail: dong.qin@mse.gatech.edu.

ORCID

Dong Qin: 0000-0001-5206-5912

Notes

The authors declare no competing financial interest.

■ ACKNOWLEDGMENTS

This work was supported in part by the National Science Foundation (CHE-1708300) and start-up funds from the Georgia Institute of Technology (GT). We acknowledge Institute of Electronics and Nanotechnology at GT for the access the Materials Characterization Facilities. L.Z. acknowledges the fellowship from the China Scholarship Council.

■ REFERENCES

(1) Willets, K. A.; Van Duyne, R. P. Localized Surface Plasmon Resonance Spectroscopy and Sensing. *Annu. Rev. Phys. Chem.* **2007**, *58*, 267−297.

(2) Jain, P. K.; Huang, X.; El-Sayed, I. H.; El-Sayed, M. A. Noble Metals on the Nanoscale: Optical and Photothermal Properties and Some Applications in Imaging, Sensing, Biology, and Medicine. *Acc. Chem. Res.* **2008**, *41*, 1578−1586.

(3) Haes, A. J.; Haynes, C. L.; McFarland, A. D.; Schatz, G. C.; Van Duyne, R. P.; Zou, S. Plasmonic Materials for Surface-Enhanced Sensing and Spectroscopy. *MRS Bull.* **2005**, *30*, 368−375.

(4) Jones, M. R.; Osberg, K. D.; Macfarlane, R. J.; Langille, M. R.; Mirkin, C. A. Templated Techniques for the Synthesis and Assembly of Plasmonic Nanostructures. *Chem. Rev.* **2011**, *111*, 3736−3827.

(5) Rycenga, M.; Cobley, C. M.; Zeng, J.; Li, W.; Moran, C. H.; Zhang, Q.; Qin, D.; Xia, Y. Controlling the Synthesis and Assembly of Silver Nanostructures for Plasmonic Applications. *Chem. Rev.* **2011**, *111*, 3669−3712.

(6) McLellan, J. M.; Li, Z.-Y.; Siekkinen, A. R.; Xia, Y. The SERS Activity of a Supported Ag Nanocube Strongly Depends on its Orientation Relative to Laser Polarization. *Nano Lett.* **2007**, *7*, 1013−1017.

(7) Xia, X.; Zeng, J.; McDearmon, B.; Zheng, Y.; Li, Q.; Xia, Y. Silver Nanocrystals with Concave Surfaces and Their Optical and Surface-Enhanced Raman Scattering Properties. *Angew. Chem., Int. Ed.* **2011**, *50*, 12542−12546.

(8) Tao, A.; Sinsermsuksakul, P.; Yang, P. Tunable Plasmonic Lattices of Silver Nanocrystals. *Nat. Nanotechnol.* **2007**, *2*, 435.

(9) Pastoriza-Santos, I.; Liz-Marzán, L. M. Colloidal Silver Nanoplates. State of the Art and Future Challenges. *J. Mater. Chem.* **2008**, *18*, 1724−1737.

(10) Millstone, J. E.; Hurst, S. J.; Métraux, G. S.; Cutler, J. I.; Mirkin, C. A. Colloidal Gold and Silver Triangular Nanoprisms. *Small* **2009**, *5*, 646−664.

(11) Wu, Y.; Sun, X.; Yang, Y.; Li, J.; Zhang, Y.; Qin, D. Enriching Silver Nanocrystals with a Second Noble Metal. *Acc. Chem. Res.* **2017**, *50*, 1774−1784.

(12) Gao, C.; Lu, Z.; Liu, Y.; Zhang, Q.; Chi, M.; Cheng, Q.; Yin, Y. Highly stable silver nanoplates for surface plasmon resonance biosensing. *Angew. Chem., Int. Ed.* **2012**, *51*, 5629−33.

(13) Sanedrin, R. G.; Georganopoulou, D. G.; Park, S.; Mirkin, C. A. Seed-Mediated Growth of Bimetallic Prisms. *Adv. Mater.* **2005**, *17*, 1027−1031.

(14) Shahjamali, M. M.; Bosman, M.; Cao, S.; Huang, X.; Saadat, S.; Martinsson, E.; Aili, D.; Tay, Y. Y.; Liedberg, B.; Loo, S. C. J.; Zhang, H.; Boey, F.; Xue, C. Coating of Silver Nanoprisms. *Adv. Funct. Mater.* **2012**, *22*, 849−854.

(15) Murshid, N.; Gourevich, I.; Coombs, N.; Kitaev, V. Gold Plating of Silver Nanoparticles for Superior Stability and Preserved Plasmonic and Sensing Properties. *Chem. Commun.* **2013**, *49*, 11355−11357.

(16) Yang, Y.; Liu, J.; Fu, Z.-W.; Qin, D. Galvanic Replacement-Free Deposition of Au on Ag for Core-Shell Nanocubes with Enhanced Chemical Stability and SERS Activity. *J. Am. Chem. Soc.* **2014**, *136*, 8153−8156.

(17) Sun, X.; Yang, Y.; Zhang, Z.; Qin, D. Mechanistic Roles of Hydroxide in Controlling the Deposition of Gold on Colloidal Silver Nanocrystals. *Chem. Mater.* **2017**, *29*, 4014−4021.

(18) Du, J.; Cullen, J. J.; Buettner, G. R. Ascorbic Acid: Chemistry, Biology and the Treatment of Cancer. *Biochim. Biophys. Acta, Rev. Cancer* **2012**, *1826*, 443−457.

(19) Wang, S.; Qian, K.; Bi, X.; Huang, W. Influence of Speciation of Aqueous HAuCl4 on the Synthesis, Structure, and Property of Au Colloids. *J. Phys. Chem. C* **2009**, *113*, 6505−6510.

(20) Goia, D.; Matijević, E. Tailoring the Particle Size of Monodispersed Colloidal Gold. *Colloids Surf., A* **1999**, *146*, 139−152.

(21) Gilroy, K. D.; Ruditskiy, A.; Peng, H.-C.; Qin, D.; Xia, Y. Bimetallic Nanocrystals: Syntheses, Properties, and Applications. *Chem. Rev.* **2016**, *116*, 10414−10472.

(22) Tan, C.; Chen, J.; Wu, X.-J.; Zhang, H. Epitaxial Growth of Hybrid Nanostructures. *Nat. Rev. Mater.* **2018**, *3*, 17089.

(23) Hickling, A.; Taylor, D. The anodic behaviour of metals. Part IV. Silver. *Discuss. Faraday Soc.* **1947**, *1*, 277−285.

(24) Sun, X.; Kim, J.; Gilroy, K. D.; Liu, J.; König, T. A. F.; Qin, D. Gold-Based Cubic Nanoboxes with Well-Defined Openings at the Corners and Ultrathin Walls Less Than Two Nanometers Thick. *ACS Nano* **2016**, *10*, 8019−8025.

DOI: 10.1021/acs.chemmater.8b04723
Chem. Mater. 2019, 31, 1057−1065

(25) Johnston, H. L.; Cuta, F.; Garrett, A. B. The Solubility of Silver Oxide in Water, in Alkali and in Alkaline Salt Solutions. The Amphoteric Character of Silver Hydroxide. *J. Am. Chem. Soc.* **1933**, *55*, 2311−2325.
(26) Zhang, J.; Winget, S. A.; Wu, Y.; Su, D.; Sun, X.; Xie, Z.-X.; Qin, D. Ag@Au Concave Cuboctahedra: A Unique Probe for Monitoring Au-Catalyzed Reduction and Oxidation Reactions by Surface-Enhanced Raman Spectroscopy. *ACS Nano* **2016**, *10*, 2607−2616.
(27) Zhang, Q.; Li, W.; Wen, L.-P.; Chen, J.; Xia, Y. Facile Synthesis of Ag Nanocubes of 30 to 70 nm in Edge Length with CF3COOAg as a Precursor. *Chem.—Eur. J.* **2010**, *16*, 10234−10239.
(28) Sambasivam, A.; Sangwai, A. V.; Sureshkumar, R. Self-Assembly of Nanoparticle-Surfactant Complexes with Rodlike Micelles: A Molecular Dynamics Study. *Langmuir* **2016**, *32*, 1214−1219.
(29) Zheng, Y.; Zhong, X.; Li, Z.; Xia, Y. Successive, Seed-Mediated Growth for the Synthesis of Single-Crystal Gold Nanospheres with Uniform Diameters Controlled in the Range of 5-150 nm. *Part. Part. Syst. Charact.* **2013**, *31*, 266−273.
(30) Chen, J.; Wiley, B.; Li, Z.-Y.; Campbell, D.; Saeki, F.; Cang, H.; Au, L.; Lee, J.; Li, X.; Xia, Y. Gold Nanocages: Engineering their Structure for Biomedical Applications. *Adv. Mater.* **2005**, *17*, 2255−2261.
(31) Yang, Y.; Zhang, Q.; Fu, Z.-W.; Qin, D. Transformation of Ag Nanocubes into Ag-Au Hollow Nanostructures with Enriched Ag Contents to Improve SERS Activity and Chemical Stability. *ACS Appl. Mater. Interfaces* **2014**, *6*, 3750−3757.
(32) Ahn, J.; Wang, D.; Ding, Y.; Zhang, J.; Qin, D. Site-Selective Carving and Co-Deposition: Transformation of Ag Nanocubes into Concave Nanocrystals Encased by Au-Ag Alloy Frames. *ACS Nano* **2017**, *12*, 298−307.
(33) Jing, H.; Wang, H. Structural Evolution of Ag-Pd Bimetallic Nanoparticles through Controlled Galvanic Replacement: Effects of Mild Reducing Agents. *Chem. Mater.* **2015**, *27*, 2172−2180.
(34) López-Tobar, E.; Hara, K.; Izquierdo-Lorenzo, I.; Sanchez-Cortes, S. Plasmonic Effects of Phenylenediisocyanides Linked at Interparticle Junctions of Metal Nanoparticles. *J. Phys. Chem. C* **2014**, *119*, 599−609.
(35) Gruenbaum, S. M.; Henney, M. H.; Kumar, S.; Zou, S. Surface-Enhanced Raman Spectroscopic Study of 1,4-Phenylene Diisocyanide Adsorbed on Gold and Platinum-Group Transition Metal Electrodes. *J. Phys. Chem. B* **2006**, *110*, 4782−4792.
(36) Bae, S. J.; Lee, C.-r.; Choi, I. S.; Hwang, C.-S.; Gong, M.-s.; Kim, K.; Joo, S.-W. Adsorption of 4-Biphenylisocyanide on Gold and Silver Nanoparticle Surfaces: Surface-Enhanced Raman Scattering Study. *J. Phys. Chem. B* **2002**, *106*, 7076−7080.

DOI: 10.1021/acs.chemmater.8b04723
Chem. Mater. 2019, 31, 1057−1065